Estuarine, Coastal and Shelf Science 270 (2022) 107839

Contents lists available at ScienceDirect

Estuarine, Coastal and Shelf Science

journal homepage: www.elsevier.com/locate/ecss

Simulation of freshwater transport network and salt flux in the Bangladesh delta

Yujuan Sun [a,*], Lucy M. Bricheno [a], Marta Payo-Payo [a], Md. Munsur Rahman [b], Neil M. Burns [c]

[a] National Oceanography Centre, Liverpool, L3 5DA, UK
[b] Institute of Water and Flood Management, Bangladesh University of Engineering and Technology, Dhaka, 1000, Bangladesh
[c] Rural Economy, Environment & Society, SRUC, Edinburgh, EH9 3JG, UK

A B S T R A C T

Circulation of saline water is important for maintaining water quality in the Ganges-Brahmaputra-Meghna (GBM) delta because of its vulnerability to the threat of climate change. We applied a numerical model to examine the volume and salt transports within the GBM delta, Bangladesh. To understand the components of salt water intrusion driven by tidal and subtidal (residual) transports, we selected 19 cross-sections to represent the complex delta circulation in a simplified network model. Our results show that over 82.51% of GBM river water drains through the eastern estuarine system (EES) in the wet season, increasing to 98.37% in the dry season. Residual transport can be comparable in size with the tidal transport in the wet season, and one order of magnitude smaller in the dry season. The western estuarine system (WES) experiences serious salinity intrusion in the dry season, and strong seasonal variability in both tidal and subtidal transport, with suppression of tide-driven transport observed during the wet season. Our results show the sub-channels area of the Lower Meghna River also faces the risk from salinity intrusion issues, as stronger tidal salt flux is estimated in the dry season. Tidal volume transport varies seasonally, corresponding to the variability of river discharge. A simplified solution by means of polynomial expansion was applied to describe the tidal propagation within river channels. Inland penetration of tidal energy is reduced with large river discharge, and additionally the propagation speed of the tidal wave increases in the wet season. Our analysis helps understand the response of the three estuarine systems to seasonal and tidal controls, and can be used to inform river management about the upstream-downstream linkages.

1. Introduction

The Ganges-Brahmaputra-Meghna (GBM) delta has the third largest freshwater discharge and is one of the most tidally dynamic deltas in the world. Freshwater from the GBM riverine system drains to the Bay of Bengal, through several estuaries along the Bangladesh coastline, bringing huge water volumes and associated sediment loads. High river discharge with strong seasonal variability, and strong tides, make the GBM delta a complex tidal-fluvial system which exhibits a mixed tidal regime and a variety of hydrodynamic regimes. The estuarine environment varies depending on the river discharge and tidal range. The western delta harbours the world's largest mangrove forest, the Sundarbans Mangrove Forest. The central delta is identified as the most important and promising farming area for prawn culture (Ahmed et al., 2008). The eastern delta includes the Padma-Lower Meghna River, which carries most of the freshwater draining to Bay of Bengal. Kida and Yamazaki (2020) found that up to 85% of GBM riverine water entered the Bay of Bengal through the Padma-Lower Meghna River. Therefore, it is necessary to examine the hydrodynamic network across the whole delta, including the flow division and salt flux transports, to understand their impacts on local agriculture, prawn cultivation, water source management and wetland ecosystem in Bangladesh.

The river discharge of the GBM riverine system is highly seasonally variable due to the monsoonal climate. The GBM river discharge can vary by over an order of magnitude between wet and dry season (Rogers and Overeem, 2017). Semi-diurnal tides are dominant in the estuaries with a strong fortnightly variation, and the tidal range decreases gradually from the Sundarbans to the Lower Meghna. In the west of the GBM delta, the tidal ranges observed along the landward boundary of the Sundarbans is up to 4 m during spring tides and 3.1 m at neap tide (Winterwerp and Giardino, 2012). These large tidal ranges cause penetration of the tidal signal far inland. For example, the Yangtze, where the mean and maximum tidal range are 2.67 and 4.62 m, and the tidal limit is as much as 630 km inland in the dry season (Zhang et al., 2012), and 350 km in the wet season (Zhang et al., 2018). A similar scenario holds for the Amazon river, where the tidal range can reach 5 m at the mouth (Rosário et al., 2009), and tides may propagate over 1000 km upstream (Kosuth et al., 2009). Elahi et al. (2020) revealed the upper limit of tidal propagation could vary between 205 km and 130 km from the estuary mouth, by changing the river discharge from 0 to 125,000 m^3s^{-1}. Strong river discharge results in high water levels in the upper river, where the decrease of tidal range has a close relationship with

* Corresponding author.
E-mail address: yujuan.sun9@gmail.com (Y. Sun).

https://doi.org/10.1016/j.ecss.2022.107839
Received 22 June 2021; Received in revised form 22 February 2022; Accepted 31 March 2022
Available online 6 April 2022

increasing river discharge compared to the river mouth (Elahi et al., 2020). Horrevoets et al. (2004) demonstrated the considerable influence of river discharge on tidal range and tidal damping primarily through friction in the upper reach of the estuary. Zhang et al. (2018) presented the maximum decrease in the amplitude of M2 could be 0.3 m from the dry to wet seasons in the Yangtze River. Savenije (2012) further demonstrated the effect of river discharge on tidal damping on changing the phage lag by causing the shift in the occurrence of high water slack (HWS), and emphasized the crucial role of the phase lag between high water (HW) and HWS on the tidal wave propagation (Savenije and Veiling, 2005). The tidal wave travels considerably slower than the classical wave phase speed when the tide is damped (Savenije and Veiling, 2005). Tidal damping increases with the upriver distance, therefore, tidal propagation can be estimated based on tidal transport and upriver distance (Kukulka and Jay, 2003a, 2003b).

Recent studies show that Bangladesh experiences a substantial water crisis due to the river diversions from the upstream Ganges (Hale et al., 2019; Kawser and Samad, 2016). Consequently, an increase of salinity was observed in its major distributary of Gorai River and its downstream streams (Shammi et al., 2012). Furthermore, the river discharge from the Ganges River will be significantly reduced, by 24%, if the proposed National River Linking Project of India is completed (Higgins et al., 2018). In the future, the GBM delta will face a more complicated and increasingly dynamic environment, particularly in the dry season. Saltwater intrusion has become a severe issue in the Sundarbans, where bulk of the saltwater is carried throughout the year (Haque et al., 2016). In a long-term process of reduced upstream discharge, the impact would cause increased saltwater intrusion in the entire GBM delta (Akter et al., 2019). A recent effect of reduced river discharge is the formation of a salt plug in the Pasur River Estuary and the export of saline water from the Shibsa River to the Pasur River through a connecting channel during the dry season (Shaha and Cho, 2016).

Flow division in tide-dominated deltas plays an important role on controlling the pathways of sediment transports, aquaculture economics and irrigation, particularly in the downstream branches (Eslami et al., 2019; Zhang et al., 2017). Complex river distributaries and narrow river channels make it very challenging for the local government to build an effective monitoring system in the Bangladesh delta, and to sustain and meet the needs of local river management, agriculture, forestry and other stakeholders. Additionally, hydrological observations in the GBM delta are not publicly accessible, are scarce and often limited to smaller regions rather than across the entire delta. In particular, two stations have been widely used in previous studies to provide daily streamflow data (Jian et al., 2009; Papa et al., 2010, 2012): the Hardinge Bridge station for the Ganges River and the Bahadurabad station for the Brahmaputra River (the latter is beyond our model domain and not used here). Therefore, the river flow distribution in the whole delta (through the numerous distributaries) remains unclear.

Based on the *in situ* river height measurements, satellite observations (TOPEX-Poseidon, ERS-2, ENVISAT, and Jason-2) are used to estimate monthly freshwater discharge of the Ganga-Brahmaputra River (Papa et al., 2010, 2012). However, this approach is limited to rivers several kilometres wide due to the spatial resolution of satellite altimeters. Another method to estimate the streamflow is using a hydrological model, but this is also limited to the major rivers in the world. Moreover, hydrological models don't generally include tidal effects, and stop landward of the salt water limit. Eslami et al. (2019) estimated the freshwater division in the Mekong Delta using the 1D model, and the simulations were further calibrated with observations. Recently, a numerical modelling approach has been widely applied in this delta (Elahi et al., 2020; Tazkia et al., 2017). Kida and Yamazaki (2020) used a two-layer model to investigate the dynamics of riverine flow in the GBM delta, while this model is simplified by only considering the main stem and one single distributary, and without tides. Elahi et al. (2020) used a two-dimensional Delft3D-FLOW numerical model to simulate the water level and current velocity in the GBM delta, and investigated the interactions between river discharge and the main tidal harmonics. Tazkia et al. (2017) studied the seasonal variation of semi-diurnal tide (M2) amplitude in the GBM delta by only considering the barotropic mode.

In this study, we conduct simulations using a state-of-the-art three-dimensional unstructured-grid ocean model, which enables the use of adaptive triangular grids to accommodate narrow and complex river channels, and a terrain-following vertical coordinate to capture water stratification in river channels and coastal regions. Our model domain includes not only the three major rivers, Ganges, Brahmaputra and Meghna, but also their large distributaries, encompassing the whole delta (Bricheno et al., 2016, 2021). Model simulations were validated and performed well allowing the calculation of volume transport and salt flux, and the calculation of tidal transport propagation across the GBM delta. From this work, a synoptic view of the salt and freshwater budget in the GBM delta is provided to inform the upstream-downstream linkage in Bangladesh river management. Our analysis improves the understanding the seasonal variation of salt flux and volume transport, and the role of the seasonal variability of river discharge on the tidal prorogation in GBM delta.

2. Materials

2.1. Model implementation

This paper used simulations from an existing state-of-the-art unstructured-grid ocean model over the Ganges-Brahmaputra-Meghna (GBM) delta, the FVCOM-GBM model hereinafter, as an extension to the work of Bricheno et al. (2016, 2021). The unstructured triangle grid provides more accurate fitting to irregular coastal geometry and makes it the best option to capture the complex geometry of narrow river channels with variable fine resolution in the riverine delta. The horizontal resolution varies from 26 km in the open ocean to 47 m within some narrow river channels inside the delta. The model uses 10 uniform sigma layers, as the bathymetry of the river channels mostly is only a few meters depth and is very well mixed in the vertical. The extent of the model grid is from inland river source at 24.0679 °N to 19 °N, and 85 °E to 93.5 °E in the east/west. Fig. 1 shows a zoom into a subarea of the wider model grid. FVCOM-GBM model was validated to show its ability to accurately reproduce tidal dynamics, and the distribution of river salinity within the GBM delta (Bricheno et al., 2016, 2021).

In this work, the simulation period was from 1st July, 2018 to 1st August, 2019, to cover the time span of *in situ* observations. The river discharge was obtained from a river Integrated Catchment model (INCA), configured for the GBM River System as a multi-reach model to provide climate projections of river flow fluxes (Whitehead et al., 2015, 2018). The combined daily river discharge, carried by the Ganges, Brahmaputra and Meghna rivers into the Bay of Bengal, was applied as one river outlet in the simulation. The location of river input was set near Hardinge Bridge on the Padma River (24.0679 °N, 89.0297 °E, marked SW90, Fig. 1). We assumed the river salinity to be 0. River water temperatures entering the delta were unknown. We examined the specific volume of water in the whole delta and conclude that water density is dominated by salinity versus temperature by a factor of ~5 (More details are provided in Appendix A). Therefore, river salinity is strongly dominant, and here river temperature was set at a constant of 22 °C. Precipitation over the entire GBM catchment has been included in the river discharge, and to avoid double counting, precipitation is not added as surface forcing separately.

Initial salinity fields and daily salinity conditions at the open boundary (along the 19 °N latitude) were obtained from the Copernicus Marine Environment Monitoring Service (CMEMS) Global Ocean 1/12° physics analysis dataset, GLOBAL_ANALYSIS_FORECAST_PHY_001_024 (Lellouche et al., 2019). Extrapolation was applied to fill inland points using the nearest three wet points. The background current field was set at 0 ms^{-1}, since the model domain was mostly inland and less influenced

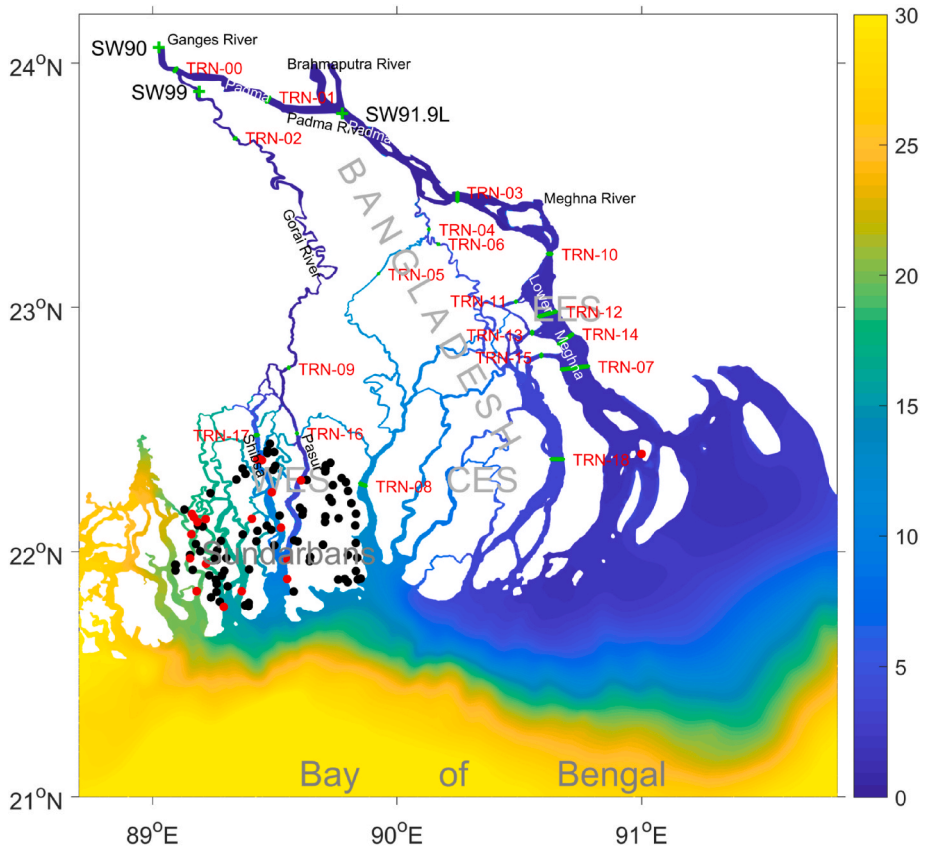

Fig. 1. Locations of all transects (green lines, TRN-00 to TRN-18), discharge stations (green crosses, SW90, SW99, and SW91.9L) and *in situ* observations (black and red dots, red dots show where observations are located within the model area). Background is the modelled annual mean surface salinity (unit: psu). (For interpretation of the references to colour in this figure legend, the reader is referred to the Web version of this article.)

by background currents in the open ocean. Tidal elevations obtained from TPXO global ocean tides model (Egbert and Erofeeva, 2002), were provided at the open boundary to address the tidal effect on the river flow. Both the temperatures of the initial and open boundary conditions were set at 22 °C, which is consistent with the setting of river temperature, as discussed in Appendix A.

2.2. Model validation

The ability of the INCA model to represent inland river discharges has been validated using gauge data on the far upstream Ganga River for the period 1981–1999 (Whitehead et al., 2015). However, our study focuses further downstream on the river systems in Bangladesh, where the measurements of river discharge are scarce. First, we examined the INCA river discharge (from July 1, 2018 to August 1, 2019) used in our model, by comparing with monthly mean observational total river discharge of the Ganges, Brahmaputra and Meghna, and the river discharge of Padma Rivers (Islam, 2016). A good agreement of seasonal variability is observed in Fig. 2a, showing high correlations over 93%. Generally, the river discharge increases rapidly in late April, and reaches a peak in August ($\sim 7 \times 10^4$ m^3s^{-1}), and then decreases from late October. The large seasonal cycle causes high river flux in the wet season (June to September), and low river flux ($\sim$2000 m^3s^{-1}) in the dry season (November to March). Compared to the climatological annual river discharge, the INCA river discharge shows a drier wet season and a drier dry season for 2018–2019.

In the GBM delta, measurements of river discharge were available at a few gauge stations (marked '+' in Fig. 1), including Hardinge Bridge station (SW90; 24.0640 °N, 89.0255 °E; 1996–2012), Gorai Railway Bridge (SW99; 23.8835 °N, 89.19 °E; 1997–2012) and Baruria Transit stations (SW91.9L; 23.7936 °N, 89.7759 °E; 1968–2012). These stations correspond to sections TRN-00, 01 and 02 in our model. We calculated the daily mean river discharge for each gauge station over their available observational time span, and made the comparisons in Fig. 2b–d. Briefly, our model results well produced the seasonal variability of river discharge in sections TRN-00, 01 and 02, showing high correlation coefficients of 79.51%, 89.24%, and 81.01% respectively. We expect the model to over-estimate flow here, due to inputting the whole catchment volume to a single point which is further upstream.

To validate salinity and density, *in situ* observations of temperature and salinity were collected in January and February 2019 as part of an aquatic biodiversity study conducted by the University of Glasgow and Shahjalal University of Science and Technology (SUST), Sylhet, Bangladesh. These data were collected at sample stations adjacent to the Permanent Sample Plots (PSPs) established by the Bangladesh Forest Department (BFD). Salinity and temperature were recorded using a multi-parameter meter (Hanna Instruments; HI-98195) deployed approximately 30 cm above the substratum at depths of 0.4–3 m. The multi-parameter meter was calibrated following the manufacturer's instructions using calibration solution (Hanna Instruments; HI9828-20) before sampling each day. Samples were collected from locations 2–4 m from the banks of channels with a variety of widths in the Sundarbans area (Fig. 1). Some of the observations were from channels not within the model mesh grids, since small streams were too small to be included.

Fig. 3a and b presents the points of observations only located within the model mesh (red dots in Fig. 1). The simulated salinity is overall slightly fresher than the observations, with mean error (MAE) of −4.12, and root-mean-square (RMS) error of 4.57 (Fig. 3a). The water density calculated from simulated salinity and temperature is also overall smaller than the density from the *in situ* observations, with MAE of −3.25 kgm^{-3} (Fig. 3b). The underestimations of model density, consistent with the underestimation of the model salinity, indicates the

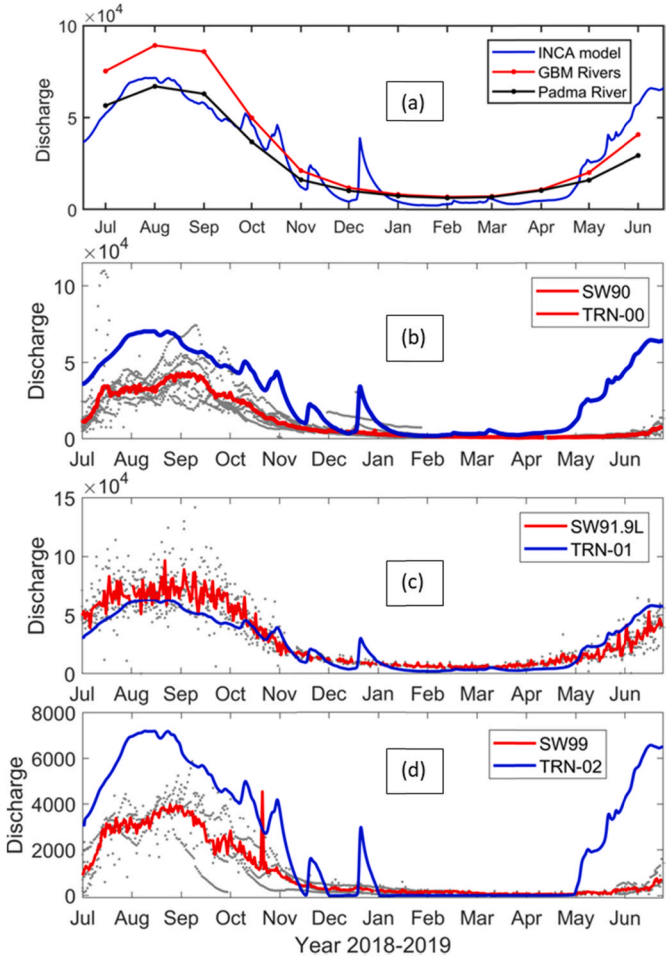

Fig. 2. Comparison of river discharge (unit: m^3s^{-1}): (a) Daily river discharge from the INCA model, monthly mean combinational discharge of GBM rivers, and discharge of Padma River obtained from Islam (2016); (b) Discharge at station SW90 and TRN-00; (c) Comparison of discharge from station SW91.9L and TRN-01; (d) Comparison of discharge from station SW99 and TRN-02. Grey dots represent the multi-years discharge measurements of each gauge station.

key role of salinity in the thermal dynamic processes within the delta. Fig. 3c shows the comparisons of density at all the available observation points, further demonstrating the dominance of salinity. The density is calculated using the same observed salinity but with different temperature, one using the observed temperature, and the other using a constant temperature as of 22 °C. A near perfect agreement is seen with correlation coefficient of close to 100%, and a very small MAE of −0.27 kgm^{-3}. Since both salinity and density have high correlation coefficients (CORR) over 90%, we believe that our model is capable of capturing the salinity and density well enough to continue with the analyses of volume and saltwater transports.

3. Calculation and methods

3.1. Simplification of riverine system

In order to calculate a freshwater budget, we designed a network of transects. The delta is divided into three sectors, the Eastern Estuarine System (EES), the Central Estuarine System (CES), and the Western Estuarine System (WES). The EES broadly represents the least saline area at the mouth of Meghna. The WES is the highest salinity area comprising the Sundarbans Mangrove Forest, and the CES is a cultivated area, which experiences strong and seasonally varying spatial gradients of salinity and is most sensitive to changes in fresh and saltwater balance. A set of 19 transects over the major river channels, is chosen to simplify this complexity into a flow network model (Fig. 4). We can use this network model to separately analyse the responses of the WES, CES and EES.

Transect 00 (TRN-00) is set next to the river input point in the model, capturing the entire freshwater flux entering the model (representative of the combined Ganges, Meghna and Bramaputra). The distribution of flow budget from the outlet of Ganges River, was examined through transects TRN-00, 01 and 02. TRN-01 is located on the Padma River, which is the main distributary of Ganges River, before it connects with the Brahmaputra River. Transect TRN-02 is located on the Gorai River, which is a distributary of the Ganges River. Freshwater flows southwards through transect TRN-02, and the sublevel transects TRN-16 on Pasur River and TRN-17 on Shibsa River, entering the Sundarbans area in the WES.

Transects TRN-03 and 04 were selected to examine the flow budget between another two distributaries: the Padma and Arial Khan River. Transects TRN-03, 10, 12, 14, and 07 are located along the main distributary of the Padma-Meghna River up to the mouth of the Meghna in the EES. Transects TRN-04, 05 and 08 represent the distributaries in the CES.

3.2. Calculation of salt flux and volume transport

Residual volume transport and salt flux transport in this study is defined as the subtidal volume transport (F_{Vr}) and subtidal salt flux (F_{Sr}), and calculated as the low-pass filtered instantaneous volume transport (F_{Vtot}) and salt flux (F_{Stot}):

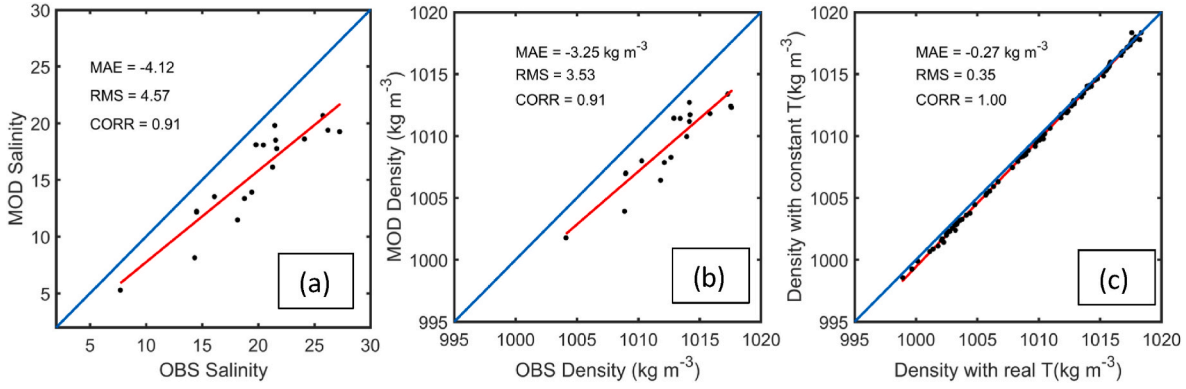

Fig. 3. Scatterplots of (a) water salinity, comparing *in situ* observed salinity and simulated salinity; (b) water density, comparing observations and simulations; (c) observational water density calculated with real temperature and with constant temperature of 22 °C.

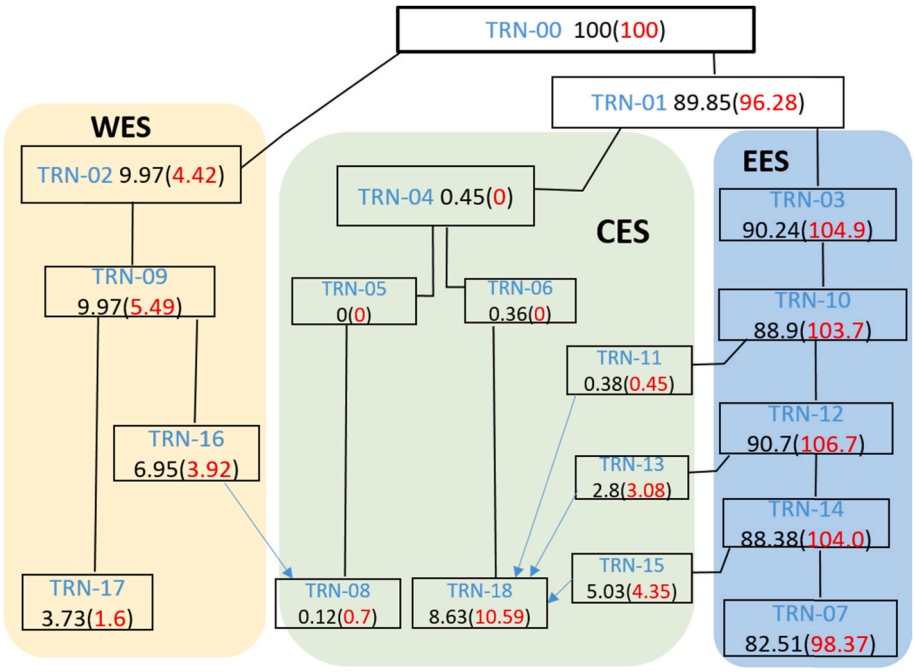

Fig. 4. Simplified River Schematic using 19 transects, and the digits represent river flow ratios (unit: %) in both wet (black colour) and dry (red colour) seasons. Blue arrows represent cross-system (east/west) river flow. All ratios are calculated relative to the river flow at TRN-00. (For interpretation of the references to colour in this figure legend, the reader is referred to the Web version of this article.)

$$F_{Vtot} = \int U^{*} \cdot dA,\ F_{Vr} = F_{Vtot},\ F_{Vtide} = F_{Vtot} - F_{Vr} \tag{E1}$$

$$F_{Stot} = \int S \cdot U^{*} \cdot dA,\ F_{Sr} = F_{Stot},\ F_{Stide} = F_{Stot} - F_{Sr} \tag{E2}$$

where dA is the sub-sectional area, $dA = (H + \xi)^{*}L$, H is bathymetry, ξ is water surface elevation, L is sub-sectional width; U^{*} is the cross-sectional velocity (calculation of U^{*} is detailed in Appendix B); S represents the salinity; the angled brackets represent a low-pass filter (here we use Godin Filter 24/25h; Godin, 1972). The Godin low-pass filter effectively removes the original tidal constituents (tidal period less than 24 h) from the hourly values (Godin, 1999). However, the compound tidal signals with slow periodicities of weeks or months cannot be removed. Low frequency compound harmonics are associated with interference cycles of, for example, M_2 and S_2 (14.77 days), K_1 and O_1 (13.66 days), and M_2 and N_2 (27.55 days). Therefore, the discharge driven by compound tides remains in the subtidal transports. Tide-induced volume transport and salt flux are represented by F_{Vtide} and F_{Stide}, hereafter called tidal (volume) transport and tidal salt flux respectively. The positive direction of volume transport and salt flux is defined as the offshore direction.

3.3. A simplified solution of tidal transports (F_{Vtide}) propagation

The mechanism of river-tide interaction is complex, here we focus on the correlation between the temporal variations in river flow and the range of F_{Vtide} along the river. We expanded the exponential expression (E3) of tidal volume transport (F_{Vtide}) along the river (Kukulka and Jay, 2003b) into a polynomial expansion (E4):

$$|F_{Vtide}(x)| = |F_{Vtide}(0)|\, e^{rx} \tag{E3}$$

$$|F_{Vtide}(x)| = |F_{Vtide}(0)| \left(1 + rx + \frac{(rx)^2}{2!} + \cdots\right) \tag{E4}$$

where, $|F_{Vtide}(0)|$ represents the amplitude of F_{Vtide} at the river mouth; r is the damping modulus (m^{-1}), which is related to the river flow, tide speed, water depth, and drag coefficient, as defined in Kukulka and Jay (2003a) with certain assumptions.

Here we use the first three leading terms on the right side of E4, and this suggests a quadratic dependence between $|F_{Vtide}(x)|$ and x:

$$R_{Vtide} = ax^2 + bx + c\ ,\ \text{where}\ \left(\frac{dR_{Vtide}}{dx}\right) < 0 \tag{E5}$$

where R_{Vtide} represents the range of tidal volume transport (F_{Vtide}). a, b, and c represent coefficients of each term, a is the tidal wave speed (ms^{-1}), b is the diffusive coefficient (m^2s^{-1}), and c is the rangeof tidal volume transport at river mouth (m^3s^{-1}). We introduce a coefficient $\gamma = \frac{b}{c}$, which physically represents the tidal damping scale of tidal volume transport. The amplitudes of F_{Vtide} can be calculated at transects (TRN-03, 10, 12, 14, and 07) along Meghna River. A simplified analytical solution was developed to estimate the tidal propagation parameters by means of the polynomial expansion.

4. Results

4.1. Freshwater volume transports

Equation (E1) was used to calculate the subtidal (F_{Vr}) and tidal (F_{Vtide}) components of volume transports, and further to estimate the river flow budget within the whole delta. The river flow ratios at the 19 transects in both dry (November–March) and wet (June–September) seasons, were calculated in respect to the river flow at TRN-00 (Fig. 4). This schematic simplifies our FVCOM-GBM model simulations into a river flow budget map, depicting the general river flow distribution in the three systems (EES, CES and WES). In the wet season, about 89.85% of river water from TRN-00 flows into the major channel, the Padma River (TRN-01), and 9.97% of freshwater flows into the Gorai River (TRN-02). Although the river discharge is general low in the dry season, we observed a higher ratio of river water (96.28%) flowing into the Padma River (TRN-01), and a lower ratio (4.42%) into the Gorai River (TRN-02). In both the CES and WES, water discharge decreases to

extreme low values during the dry season. At first sight, abnormal flow ratios (over 100%) can be seen at sections TRN-03, TRN-10, TRN-12, and TRN-14 along the Lower Meghna River, given the ratio at TRN-12 is 106.77%, reaching a total bias of over 11%. The uncertainties are attributed to the compound tidal signals which remains in the subtidal component, and strong tidal amplification occurs in the dry season (Fig. 6d).

The mean range of F_{Vtide} is defined as the difference between the largest and the smallest tidal volume transports over a tidal period averaged through a whole month. In the study period, the averaged water discharge into the Bay of Bengal was 29,512 m^3s^{-1}, with a maximum of 71,636 m^3s^{-1} during the flooding season and a minimum of 2180 m^3s^{-1} during the dry season (Table 1). Substantial river discharge and frictional dissipation stops the tide propagating beyond the confluence of the Ganges and Brahmaputra rivers (Bricheno et al., 2016). Our results (Table 1) show the same finding that no obvious tidal fluctuation of tidal volume transports (F_{Vtide}) is found at sections TRN-00, TRN-01, and TRN-02 in either the wet or dry seasons. Subtidal volume transports (F_{Vr}) show a significant seasonal variability at these three sections, stronger in the wet season than in the dry season.

In the EES, F_{Vr} along the Padma-Lower Meghna River, can reduce from 6×10^4 m^3s^{-1} in the wet season by more than one order of magnitude in dry season (3×10^3 m^3s^{-1}). The range of F_{Vtide} shows a seasonal variability, by being larger in dry season. Tidal transports dominate at sections close to the estuary mouth (like TRN-07, 08, 18), and can be as large as or greater than the residual flow. About 82.51% of river water drains to Bay of Bengal through the mouth of the lower Meghna River (TRN-07) in the wet season, while the freshwater flows through its sub-channels, TRN-11, TRN-13 and TRN-15, providing as much as 8.21% through TRN-18 into the CES.

In the CES, our model results show no flow into the distributary containing TRN-04 in February, and even in the wet season the subtidal volume transport is about 446 m^3s^{-1} (0.45%). No tidal signal was tracked at TRN-04. This underestimation of river volume transport was due to a lack of accurate bathymetry in the model. Some 'blockages' were found in this river channel, and the issue of river blockages is further addressed in the supplementary material (Appendix C). Consequently, seasonal modulation of the tide by freshwater was not evident at TRN-08. The ranges of tide-driven volume transport are large, but change very little between August and February, corresponding to 13381 and 13015 m^3s^{-1}, respectively.

In the WES, at TRN-09 upstream of the Sundarbans Mangrove Forest, the volume transport was about 7200 m^3s^{-1} in August, but as little as 10 m^3s^{-1} in February, while the amplitudes of tide-induced volume transport in February was in the order of 10^2 m^3s^{-1}, and 1 order less in August. Pasur River (TRN-16) and Shibsa River (TRN-17) are two tidal rivers in the Sundarbans area, carrying 6.95% and 3.73% of the water flow respectively. Pasur River carries almost twice the volume of the Shibsa River in August, due to its direct connection to upstream river. The amplitudes of tidal volume transport at TRN-16 are about in the order of 10^2 m^3s^{-1} in August and 10^3 m^3s^{-1} in February. However, tide-induced volume transport (F_{Vtide}) is large at TRN-17, with amplitudes in order of 10^3 m^3s^{-1} in both August and February. Attributed to the weak flow from upstream river in the dry season, the volume transport at TRN-16 is about 16 m^3s^{-1} in February, and it is −31 m^3s^{-1} at TRN-17. This reversal indicates salt intrusion in Shibsa River during the dry season.

Table 1
Mean residual volume transports (unit: m^3s^{-1}), and the mean range of tidal volume transport at 19 sections in August and February.

Sections	August		February	
	F_{Vr}	Range of F_{Vtide}	F_{Vr}	Range of F_{Vtide}
TRN-00	68,951	–	2538	–
TRN-01	62,015	–	2638	–
TRN-03	62,540	[−844; 625]	2926	[−10,000; 6376]
TRN-10	61,536	[−9411; 3836]	2909	[−21,735; 15,977]
TRN-12	62,794	[−22,509; 9746]	3039	[−33,695; 26,106]
TRN-14	61,168	[−30,597; 13,734]	2960	[−41,749; 31,546]
TRN-07	57,139	[−40,175; 20,493]	2862	[−52,697; 40,320]
TRN-02	7036	–	0	–
TRN-09	7256	[−51; 33]	10	[−716; 598]
TRN-16	4991	[−255; 174]	16	[−1288; 934]
TRN-17	2683	[−4146; 2380]	−31	[−3300; 2963]
TRN-04	446	–	0	–
TRN-05	0	–	0	–
TRN-06	361	–	0	–
TRN-08	104	[−8043; 5338]	61	[−7802; 5218]
TRN-11	231	[−861; 1600]	14	[−1082; 1403]
TRN-13	1991	[−688; 1477]	83	[−1251; 1800]
TRN-15	3534	[−3873; 4736]	24	[−3617; 4464]
TRN-18	6100	[−10,770; 51,65]	376	[−9216; 7725]

4.2. Tidal transports propagation in Meghna River

At section TRN-03 (140 km upstream from the mouth of the Lower Meghna, 91°E, 22.4°N), tidal volume transport was calculated, with a mean range of 1469 m^3s^{-1} in August and 16376 m^3s^{-1} in February. The seasonal variation in F_{Vr} was over one order of magnitude (due to the dramatic drop of the river discharge) and varied between 62540 m^3s^{-1} in August and only 2926 m^3s^{-1} in February. The fluctuations of F_{Vtide} are larger in February than in August, showing the modulation of tidal propagation in the presence of river discharge. The decrease in the tidal volume transport has a positive correlation with increasing river discharge (agreeing with the results of Elahi et al., 2020). Closer to the estuary mouth (from TRN-03 through TRN-07), the tidal signals become stronger in both August and February. Fig. 5a presents the monthly mean range of F_{Vtide} at sections TRN-07, 14, 12, 10 and 03, which are about 48 km, 61 km, 75 km, 99 km, and 140 km upstream from the estuary mouth of the Lower Meghna River (91°E, 22.4°N). The variations of the F_{Vtide} range in different months show a consistent trend along the upstream distances: the further upstream from the river mouth, the smaller F_{Vtide} range is. This shows the effect of tidal damping in the tidal wave propagation and indicates that the range of F_{Vtide} is correlated to the upstream distance (x).

Best-fit approximations of tidal volume transport range from E5 (Fig. 5b), were almost identical to our simulations, with averaged root-mean-square error of 6×10^{-11} m^3s^{-1}, and correlation coefficient of 99.96%. Tidal limits can be estimated using $\frac{dR_{Vtide}}{dx} = 2ax + b = 0$, and the monthly mean are presented in Fig. 6b with the origin of river mouth setting at (91 °E, 22.4 °N). The tidal limit could reach up to 174 km in November, while tidal propagation stops at 147 km in August. Estimations of the coefficients a and γ in E5 (Fig. 6c–d respectively) show the annual variation of strong seasonal variability corresponded to the river flow discharge. Both tidal wave speed a and tidal damping coefficient γ depend on the river flow discharge and tidal transport: a has a positive correlation with river discharge and a negative correlation with tidal transport, while γ shows the reverse. Both a and γ have stable spatial correlations with river discharge, of 83% and −98% respectively, while the correlation between a (or γ) and tidal volume transport varies spatially, with a smaller correlation coefficient of −80% (97.8%) near the river mouth, and the highest correlation of −89% (99.5%) at TRN-10, due to the strongest tidal amplification there (Fig. 6e). The tidal amplification factor is calculated as the ratio of tidal range between upstream transects and downstream TRN-07 (Wang et al., 2019). Generally, high river discharge corresponds to a lower range of tidal volume transport and weaker tidal amplification. In the dry (wet) season, tidal amplification (attenuation) gradually increases with range of tidal volume transport, which decreases (increases) as the tidal wave travels upstream. The strongest tidal attenuation (amplification factor less than 1) occurs at TRN-03 in the wet season, but shows no amplification or attenuation from January to April. Tidal attenuation can be seen at TRN-10, 12, and 14 in August. At TRN-10 tidal amplification

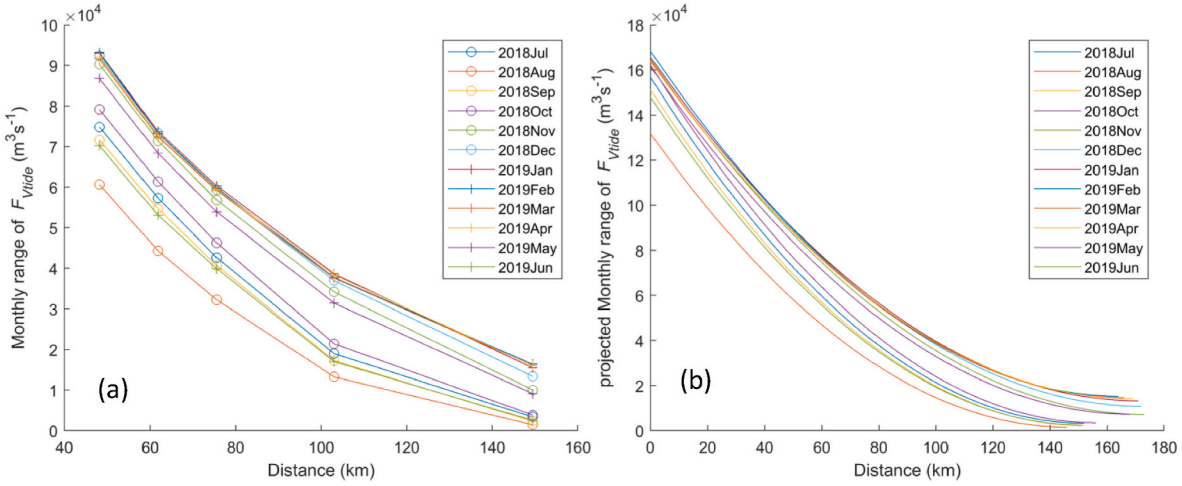

Fig. 5. (a) Monthly mean range of tide-driven volume transports along Lower Meghna River, and the distance is calculated from the estuary mouth (91 °E, 22.4 °N); (b) Approximation of the range of tidal volume transports.

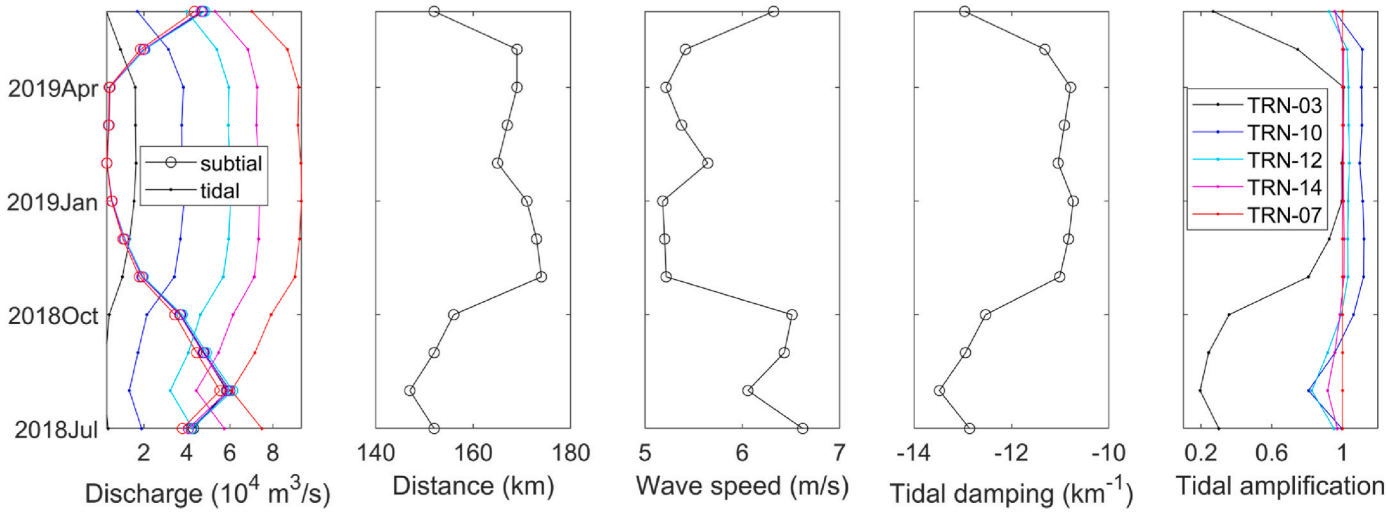

Fig. 6. (a) Monthly mean subtidal transports (circle-line), and range of tidal transports (dot-line) at transects (represented by different colours as in d); (b) tidal limits (km); (c) parameter a, wave speed (ms^{-1}); (d) parameter γ, tidal damping (km^{-1}); (e) tidal amplification factor at transects, defined as the ratio of tidal range between the other transects and TRN-07. (For interpretation of the references to colour in this figure legend, the reader is referred to the Web version of this article.)

(larger than 1) is apparent from October through next May (dry season), and this is caused by the narrowing and deepening river channel there.

Clear seasonal variation in wave propagation speed and tidal damping coefficient was observed. Tidal wave speed is faster in the wet season (June to October) than that in the dry season (November to May). This could be related to the change in water depth, assuming as the classical wave phase speed $\sqrt{gh}$, that water depth increases in the wet season due to the high river discharge. Stronger tidal damping occurs in August (Fig. 6d), resulting in the slower wave speed than other wet months (Fig. 6c). However, this is not applicable to the reinforced wave speed in February as tidal damping increases slightly than other dry months. Due to the prominent river discharge in August (larger than the amplitudes of F_{Vtide}), there is no occurrence of HWS, i.e. water always moves offshore. Our simulation shows a shift of phase lag in February, with phase lags increasing by as much as 7.3° compared to both January and March. Therefore, the suppression and reinforcement of tidal wave speed in August and February, are attributed to the combined effect of the phase lag and the balance between friction and convergence.

4.3. Salinity at transects

Fig. 7 presents the time series of salinity at sections in EES (TRN-03, 10, 12, 14, 07), CES (TRN-08, 11, 13, 15, 18), and WES (TRN-16, 17), from 1st August, 2018 through 1st August, 2019. Table 2 displays the mean salinity and the range of salinity caused by tidal fluctuations in August and February. Salt intrusion starts in November with the arrival of the dry season, and there is a dramatic freshening driven by the arrival of the monsoon in May. Generally, annual variation of salinity in the river channels within the delta is controlled by the monsoon, maintaining relative low values in the wet season, and higher values in the dry season.

In the EES (Fig. 7a), the salinity at TRN-03 was low throughout the year, while at the downstream sections, the salinity increased to about 0.8 in wet season, and 2.2 in dry season. The ranges of salinity fluctuation caused by tidal effect are small, remaining within magnitudes of 10^{-2}. A significant freshening was observed in December 2018 at sections TRN-10, 12, 14, and 07, corresponding to a sudden spike of freshwater discharge (see Fig. 2).

In the CES, salinity at TRN-08 kept a stable high value of 12.8 throughout the simulation period, which was caused by the low river

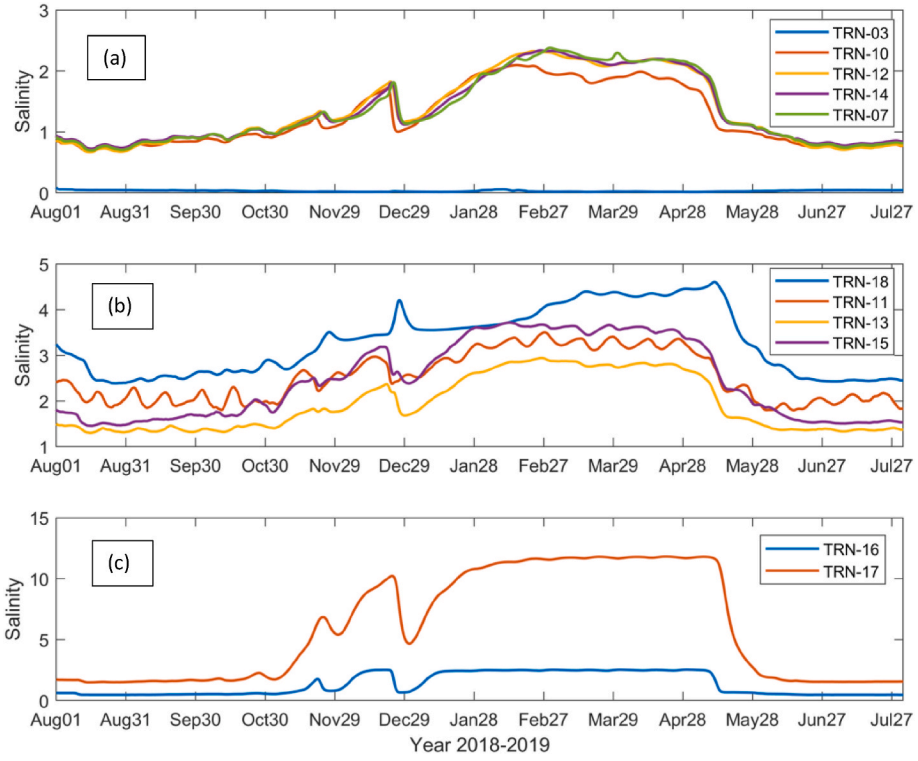

Fig. 7. Time series of salinity (unit: psu) at the sections in the three systems (a) EES, (b) CES, and (c) WES.

Table 2
Mean salinity and the range of tide-driven salinity fluctuations in August 2018 and February 2019.

Sections	August		February	
	$Salinity_r$	$Salinity_{tide}$	$Salinity_r$	$Salinity_{tide}$
TRN-03	0.05	–	0.04	−0.02, 0.07
TRN-10	0.75	−0.03, 0.02	2.05	−0.02, 0.02
TRN-12	0.74	−0.02, 0.02	2.21	−0.01, 0.02
TRN-14	0.80	−0.03, 0.02	2.16	−0.01, 0.01
TRN-07	0.77	−0.03, 0.03	2.14	−0.04, 0.04
TRN-08	12.82	−0.18, 0.16	12.83	−0.14, 0.12
TRN-11	2.13	−0.49, 0.45	3.30	−0.63, 0.51
TRN-13	1.38	−0.14, 0.08	2.83	−0.1, 0.1
TRN-15	1.57	−0.04, 0.07	3.65	−0.13, 0.19
TRN-18	2.69	−0.02, 0.02	3.79	−0.04, 0.06
TRN-16	0.52	−0.004, 0.004	2.49	−0.14, 0.13
TRN-17	1.58	−0.1, 0.2	11.40	−0.12, 0.17

water discharge flowing into this river channel (104 m^3s^{-1} in August). However, the large range of tide-driven volume transports reached 13381 m^3s^{-1} in August, making TRN-08 effectively a saline water dominant environment. The range of tide-induced salinity fluctuations ranged from 0.34 in August and 0.26 in February in EES. Sections on the sub-channels of the Lower Meghna River (TRN-11, 13, 15) have relatively higher values of salinity than that in the main stream in both August and February, 1.38–2.13 and 2.83–3.65 respectively. Tidal effect on salinity was observed strongest at TRN-11, where salinity varies between 0.94 in August, and 1.14 in February. Relatively strong tidal influence on salinity was also seen at TRN-13 and TRN-15, changing from 0.22 to 0.11 in August, to 0.2 and 0.32 in February, respectively. The strong tidal influence at TRN-11 was mostly attributed to the low river discharge (231 m^3s^{-1} in August), compared with 1991 m^3s^{-1} and 3534 m^3s^{-1} at TRN-13 and TRN-15.

In the WES, salinity at TRN-16 and 17 showed a similar annual variability to the rest of the delta, with corresponding increases of salinity in November, and freshening as a consequence of pulses of river discharge input. However, the salinity at TRN-17 (Shibsa River) was significantly higher than that at TRN-16 (Pasur River), especially in the dry season. The salinity at TRN-17 increased from 1.5 in flood water season to 11.8 in low water season, showing the severe salt water intrusion in the Shibsa River Estuary. Pasur River (TRN-16) carries more freshwater than Shibsa River because of its direct connection with the upstream main source, resulting in a low salinity of 0.5 in dry season and 2.5 in wet season.

4.4. Salt flux transports

The local salinity values and volume transports are now combined to calculate salt transports throughout the GBM delta. Table 3 presents F_{Sr} and the range of F_{Stide} in August 2018 and February 2019 (defined in E2). Fig. 8 presents the time series of tidal and subtidal salt flux at TRN-07, 08 and 16, which allows us to picture the annual variations of salt flux at the estuary mouth from east to west in the delta.

Table 3
Monthly mean Salt Flux (unit: psu m^3s^{-1}) and its tide-driven fluctuation in August and February. Note negative F_{Sr} indicates a net salt intrusion.

Sections	August		February	
	F_{Sr}	Range of F_{Stide}	F_{Sr}	Range of F_{Stide}
TRN-10	45,769	−7610; 3894	5873	−44,377; 32,636
TRN-12	50,142	−17,837; 8009	6816	−73,879; 57,305
TRN-14	48,312	−23,597; 11,062	6572	−89,559; 67,989
TRN-07	44,807	−31,457; 16,579	6519	−115,154; 89,050
TRN-08	1374	−102,077; 68,594	843	−99,215; 66,468
TRN-11	409	−1888; 3343	−44	−3812; 4685
TRN-13	2841	−917; 1925	240	−3597; 5222
TRN-15	5312	−5805; 6938	51	−13,077; 15,770
TRN-18	16,465	−28,936; 13,808	1452	−34,280; 28,700
TRN-16	3955	−331; 250	−149	−3885; 2548
TRN-17	4411	−6720; 3816	−392	−37,398; 34,068

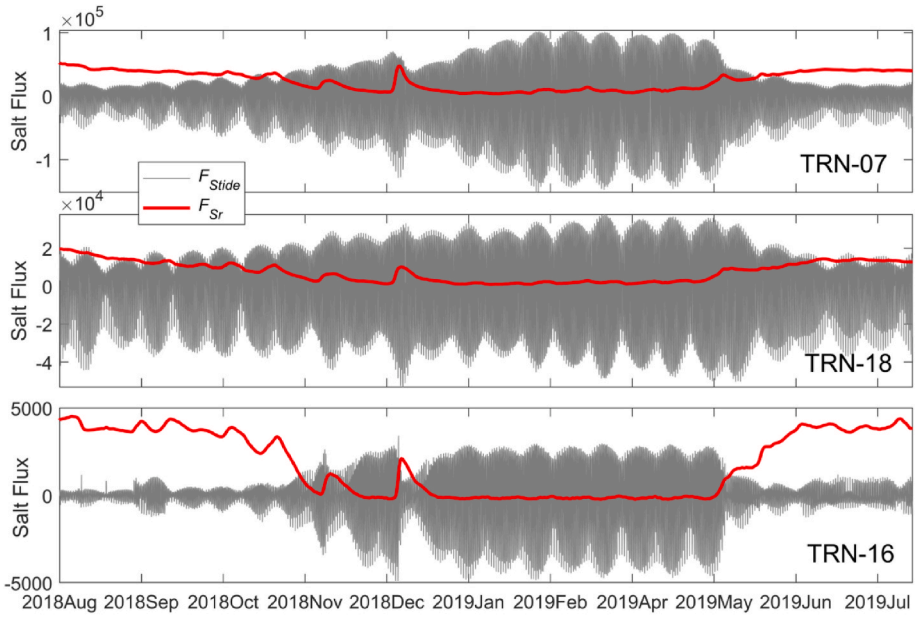

Fig. 8. Annual variations of tidal salt flux (grey line) and subtidal salt flux (red line) at TRN-07, 18 and 16. (For interpretation of the references to colour in this figure legend, the reader is referred to the Web version of this article.)

In the EES, salt flux transports at TRN-10, 12, 14, and 07 were strong, in order of 10^4 *psu*m^3s^{-1} in August and 10^3 *psu*m^3s^{-1} in February (Table 3). F_{Stide} increases along the downstream sections in both dry and wet seasons. Although the salinity increased by about 1.4 in the dry season compared to the wet season, the mean F_{Sr} were smaller due to the combination of dramatic decreasing of river discharge and strengthened tidal effect. Taking TRN-07 for example, in the wet season, due to high river discharge, the range of F_{Stide} is relatively small, and F_{Sr} is always larger than F_{Stide}; in the dry season, the amplitude of F_{Stide} increases as the river discharge decreases and tidal energy is able to penetrate further inland.

In the WES, saline water intrusion can be observed at both TRN-17 (Shiba River) and TRN-16 (Pasur River) during the dry season, with F_{Sr} of −392 and −149 psum^{3}s^{-1} respectively. Negative numbers indicate flooding-tide direction and hence a landward salt intrusion. Annual variation of salt flux at TRN-16 (Fig. 8) is similar to that at TRN-07. Both tidal and subtidal salt flux have strong seasonal variability, showing again the suppression of tidally driven transports during periods of high river discharge. A spike of river discharge in December further demonstrated the control of river forcing on both tidal salt flux and volume transports.

In the CES, salt fluxes calculated at TRN-08 were thought to be unreliable, due to inaccuracies in the model bathymetry. While F_{Stide} at TRN-18 is in magnitude of 10^4 during both the dry and wet season (Table 3), and the F_{Stide} is comparable to F_{Sr} even in the wet season (Fig. 8), indicating TRN-18 is at risk of saline water intrusion in the future. Tidal-induced salinity fluctuations were strong at TRN-11, with F_{Sr} of −44 psum^{3}s^{-1} in February, which means the salt flux transport is in the direction towards the main freshwater source – Lower Meghna River. A low F_{Sr} salt flux of 51 psum^{3}s^{-1} with a much stronger tidal salt flux (10^4) in February can be seen at TRN-15, implying that these subchannels area of Lower Meghna River are at greater risk from intrusion issues in the future.

5. Discussion

We built a river schematic network (Fig. 4) to constrain the volume and salt transport budget quantitatively in a tide-dominated megadelta characterized by the complex distributaries and multiple-channel estuary. The GBM delta can be categorised together with other tide-dominated deltas, such as the Yangtze and Mekong deltas (Zhang et al., 2018; Eslami et al., 2019). However, the GBM delta shows large river discharge variations which are strongly controlled by the seasonal monsoon climate. Also, tidal propagation and salt intrusion change seasonally in response to the discharge variations due to raised water levels, and increased non-tidal current speed. The morphology of these three deltas is also very different. The Mekong divides into seven branches and the Yangtze just two before emptying into the sea. Compared to this, the GBM delta has a more complex channel network. The Mekong delta is a multi-channel estuarine system, with the river flow fractions of the branches at the river mouths range from 6% to 23.8% (Eslami et al., 2019). Therefore, the flow in these channels is more equally distributed across the Mekong delta. Our results show a large difference in river flow fractions among the branches, like 98% in EES and 5.52% in WES during the dry season, reflecting the different hydrodynamic processes exist across the GBM delta. Another important difference is the range of tidal conditions that exist across the delta. With large amplitude tides at the northeast and northwest corners of the Bay of Bengal. This unique combination of tidal and river forcing, means that a range of conditions are experiencing in the GBM delta. Some areas experiencing high flow and high tide (EES) while the WES experiences high tide and low discharge. The CES experiences a reduced tide, but also receives a large discharge. In this respect, different sections of the GBM delta could be classified separately – hence it is an unrivalled location to study interactions of river and tide controlling transport within a delta.

We calculated the tidal prisms using the method in Rynne (2016) and display the ratios of tidal prisms and freshwater in spring/neap tides during the dry/wet season in Table 4. Generally, these ratios show larger values in Spring Tide than that in Neap Tide. During the wet season, the ratios are in smaller values (less than 1), that the freshwater discharge is larger than tidal prism, particularly at TRN16 in the WES. However,

Table 4
Ratios of the tidal prism and freshwater transport.

	Wet-Spring	Wet-Neap	Dry-Spring	Dry-Neap
TRN-07 (EES)	0.4	0.2	10.4	8.2
TRN-16 (WES)	0.05	0.02	75.4	34.5
TRN-18 (CES)	1.0	0.4	18.5	12.4

during the dry season, the ratios are large values, the largest in WES, then CES and EES, due to the reduced river water and the strengthened tidal effect in the dry season. At TRN16, the ratios can be up to 34.5 in Neap Tide and even to 75.4 in Spring tide, indicating the dominance of the tidal prism in the WES during the dry season, accounting for the severe saline intrusion there. The tidal prism is over 12–18 times of the freshwater volume in the CES, indicating that the potential increasing risk of saline intrusion in CES.

Thus, we partitioned the GBM delta into three estuarine systems with respect to the flow division, to assert different hydrodynamic processes in the EES, CES, and WES respectively. This work has allowed us to investigate how the three contrasting regions interact, and aids understanding of the upstream-downstream linkage in hydrological processes and river management across the GBM delta. Particularly in the CES, although both TRN-08 and 18 enter the Bay of Bengal at similar latitudes, they behave differently. TRN-18 carries about 8% of the total freshwater from the upstream sub-channels (TRN-11, 13 and 15) connecting the EES and CES, making it more fluvial dominant, with slight fluctuations of the salinity (~1) from wet to dry season. TRN-08 is slightly unreliable owing to the blockage in the upstream, and we believe this to be an issue with river connectivity in the model and not a real feature. There is no freshwater coming down through TRN-05, which is why there is no seasonal variability in TRN-08, where salinity is high (of 12.8) all year round and both tidal volume transport and salt flux are stable. This has been identified as an area for improvements. One experiment has been conducted by replacing the bathymetry of dry points by the averaged bathymetry of its surrounding wet points (see Appendix C for more details), showing a better connectivity in CES. However, using modified bathymetry adds additional freshwater to the WES, and unrealistically reduces the salinity in the Sundarbans, so increases the bias here. In this study, we used the original bathymetry (based more closely to observations) for all our analysis, as the bathymetry uncertainty is crucial for the tidal current speed calibration in a meso-tidal estuary (Cea and French, 2012). But in future studies, it may be useful to modify the bathymetry in the CES only and leave the WES unaffected. Using this approach, we could develop the improved bathymetry inferences based on the river flow behaviour in deltas which lack accurate measurements of bathymetry.

Subtidal components of volume transports and salt flux tend to be strong in wet seasons and weak in dry seasons, while the amplitudes of tidal components are larger in the dry seasons. This is because the 'competition' between tide and river is reduced, and the tidal energy can penetrate further in land during periods of low discharge. However, in wet seasons the river flow is large, with fast velocities in the offshore direction and high associated water levels. This offshore flow acts in opposition to the incoming tidal force, supressing the tidal range, and stopping the tidal energy penetrating as far inland. In this way, we see the combined impact of tidal-river interaction on the change in tidal wave speed as the tidal wave travels upstream. The work of Bricheno et al. (2021) showed that the seasonal excursion is around 5 times the distance of the tidal excursion, demonstrating that the salt intrusion length is more dependent on the seasonal variation of the river discharge. Furthermore, the rising sea levels also can enhance the salinity intrusion, as the sea level rise can increase the tidal range and therefore exacerbate salt intrusion.

The subtidal salt flux can be further decomposed into three components, transports caused by the freshwater flow, the residual shear flow (cross-sectional varying), and by the net effect of tidal oscillation (Bowen et al., 2003; Lerczak et al., 2006). We used the method of Lerczak et al. (2006) to calculate these three components and found salt flux due to the freshwater flow was dominant, and the other two components of subtidal salt flux occupied only a small fraction, attributed to the fluctuations of the subtidal salt flux in dry season. Therefore, the decomposition of the salt flux into tidal and subtidal components in this study, has provided the overall flux estimates of salt water intrusion across the whole delta. There is no need to further decompose the subtidal salt flux.

6. Conclusion

In this study, we summarised the river flow and circulation of salinity across 19 transects in the GBM delta, into a simplified network model, and demonstrate the differing behaviour across three contrasting delta regions (EES, CES, and WES). Our results show that 82.51% of freshwater in the wet season drains to the Bay of Bengal through the EES, increasing to 98.37% in the dry season. The results also reveal the vulnerability of the three estuarine systems to salinity intrusion: the most vulnerable region is the Sundarbans area (WES), then is CES, and the least vulnerable is EES, which agrees well with the conclusion from Murshed et al. (2019). The large range of F_{Sr} and strong F_{Stide} seen in the cross-channel sections (particularly TRN-15), suggests that these sub-channels areas of Lower Meghna River should be further investigated for the saline water intrusion issues in the future.

By fitting the range of tidal transports in a quadratic function to the distance from estuary mouth, our results present a clear seasonal variation of the tidal damping coefficient, tidal wave speed, and tidal limits. Low river discharge corresponds to a larger range of tidal transport and a stronger tidal amplification in the dry season. Tidal wave speed is lower in dry season, and higher in wet season, as a result of water depth controlling the phase speed of the tidal wave. However in addition to clear seasonal variation, the tidal wave speed is observed to be reinforced (or suppressed) in the February (or August), attributed to the phase lag between high water and high water slack, and the balance between friction and convergence. This simplified solution has allowed us to understand the mechanisms through which river discharge can both enhance and supress tidal propagation.

Changes in future tidal behaviour may impact freshwater availability on the deltas globally. River flow and salt budgets calculated in this work can be extended to estimate the distribution of river flow in other deltas, for any river discharge under the challenges of future climate change and water security scenarios. The proportion of river water draining into the Bay of Bengal through several estuary mouths could be estimated under different scenarios, providing more accurate river input values to regional Bay of Bengal offshore models. The simplified river flow network model can provide a proxy to estimate the sediment transport in the complex GBM delta. The next step will be to combine the approach outlined here with the future scenarios in Bricheno et al. (2021). By analysing the response of volume and salt-fluxes to future sea-level rise and variability of river discharge, we can contextualise this one-year study with the inter-annual variability of the GBM delta in response to climate change by end of this century.

CRediT authorship contribution statement

Yujuan Sun: Conceptualization, Data curation, Investigation, Methodology, Resources, Formal analysis, Software, Validation, Visualization, Writing – original draft, Writing – review & editing. **Lucy M. Bricheno:** Conceptualization, Methodology, Writing – review & editing, Validation, Supervision. **Marta Payo-Payo:** Methodology, Writing – review & editing. **Md. Munsur Rahman:** Writing – review & editing, Supervision, Investigation. **Neil M. Burns:** Data curation, Investigation, Writing – review & editing.

Declaration of competing interest

The authors declare that they have no known competing financial interests or personal relationships that could have appeared to influence the work reported in this paper.

Acknowledgement

This work is supported by project ACCORD, which is funded by the

Natural Environment Research Council (NERC) and the Global Challenges Research Fund (GCRF) as part of a National Capability Official Development Assistance award, NE/R000123/1. The *in situ* observations were collected as part of a NERC Global Partnerships Seedcorn Fund project, NE/S008233/1. Dr Yujuan Sun acknowledges the support from the project funded by UK-Canada Arctic Bursaries 2020 during the revision process. We sincerely acknowledge the work of Dr Jason T Holt and Dr Sarah L Wakelin for their preview comments and suggestions, and the work of Dr David M Bailey, Dr Swapan Kumar Sarker and Dr Charlotte R Hopkins for their contribution of the *in situ* data collection, and thank the Bangladesh Forest Department for providing logistic support during fieldwork. We acknowledge the funding from UKRI via grant EP/R024480/2 for supporting Dr Marta Payo Payo, and the projects ESPA Deltas (NE/J002755/1) and DECCMA (Grant no. IDRC 107642) for supporting Dr Munsur Rahman.

Appendix A. Dominant Salinity in river channels

Water temperature is a critical parameter to assess the physical and thermal dynamics in both the coastal area and the deep ocean. However, in the Bangladesh riverine system, the river water lacks temperature observations with which to force and validate our model. The salinity of freshwater is usually treated as 0, which is far less than the sea salinity. Considering this large difference in salinity, the contribution of both temperature (T) and salinity (S) in density estimation is examined from

$$\Delta_{S,T} = \alpha(S,T,0) - \alpha(S_0,T_0,0)$$

$$\alpha(S,T,0) = 1/\rho(S,T,0)$$

$$S_0 = 35;\ T_0 = 0$$

where, $\alpha(S,T,0)$ is the *Specific volume* at surface (depth = 0), with unit m^3kg^{-1} ; $\Delta_{S,T}$ is the *thermosteric anomaly*, which can be expressed as a simple linear equation to estimate the contribution of salinity and temperature:

$$\Delta_{S,T} = A\delta_T + B\delta_S + C$$

$$\delta_s = S - S_0;\ \delta_T = T - T_0$$

Here we use the *in situ* temperature and salinity collected within Bangladesh delta (mentioned in Section 3.2), thus, the coefficients for each term can be calculated: $A = 2.52 \times 10^{-7}$; $B = -7.44 \times 10^{-7}$; $C = -2.02 \times 10^{-6}$. Figure A1 shows the ratio of the contribution from salinity ($B\delta_S$) and from temperature ($A\delta_T$), accounting for the density simulation in September, addressing that the dominant role of Salinity within the Bangladesh delta, of about 5 times more than temperature, while the dominant role of salinity reduces offshore.

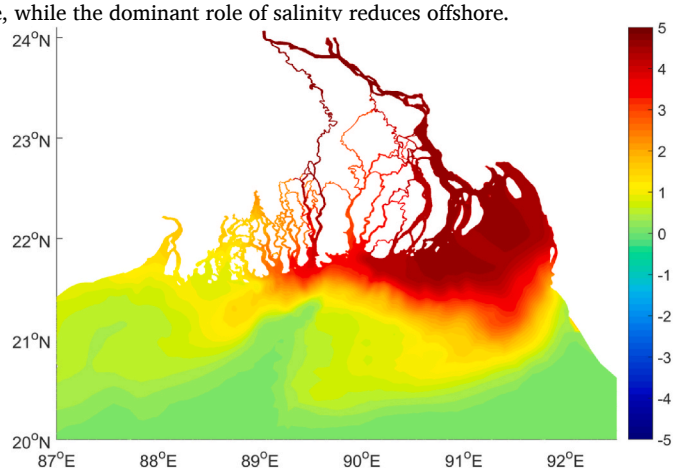

Fig. A1. Ratio of contribution of Salinity and Temperature to Density

Appendix B. Calculation of cross-sectional velocity

To calculate the cross-sectional velocity, a new coordinate system (σ,λ,z) was introduced at each section, where σ and λ represent along-section and across-section directions, respectively. The setup of new coordinate system is conducted in three steps. Firstly, to obtain the velocity (U_0 V_0) at the selected reference point, where the velocity direction is (or is nearly) parallel to the river channel. Secondly, draw the line of transect, which is perpendicular to the velocity direction at the reference point, obtaining the two intersections where the transect line meets the river banks and determine geographic coordinates of a number of points on the transect line. Thirdly, to calculate the cross-sectional velocity (U^*) using the simulated northward and eastward velocity (U V) at each point:

$U^* = \sqrt{U^2 + V^2}*\cos(\theta - \alpha)$, where $(\theta - \alpha)$ represents the angle between (U V) and (U_0 V_0), $\tan\alpha = V_0/U_0$, $\tan\theta = V/U$.

For complex river channels, where the bathymetry at sections is relatively shallow, we further simplify the calculation by using the depth-averaged velocity and salinity, which are spatially varying only along the σ direction, corresponding to $U^*(\sigma,t)$ and $S(\sigma,t)$.

Appendix C. River connectivity

The distinctive geography of the Bangladesh delta, consisting of both the low-lying floodplain and the tidal delta, increases the vulnerability of the water-land conversions in response to the impacts of human- and climate-induced changes (Donchyts et al., 2016). Due to changes in meanders, it is hard to obtain accurate bathymetry for the model. In the original model (Bricheno et al., 2016), the bathymetry was obtained from both the existing surveys and new river channel surveys performed during 2013/14, capturing the best possible description of the nearshore and inland bathymetry over the estuary. However, some dry points are found in the narrow river channels within the delta, where the bathymetry is above the water level, and blocks the river freshwater flows into the downstream channels. An efficient method to improve the connectivity of river channels might be to modify the bathymetry of the dry points, although there are no observation data from extra surveys. The method applied in this study is to replace the bathymetry of dry points by the averaged bathymetry of the surrounding wet grid. For example, the red color in Figure C1a represents the original bathymetry of the dry points (higher than 0 m). Figure C1b shows the modified bathymetry, with the bathymetry at the original dry points below the water level (less than 0 m).

Figure C2a gives a snap-shot of model surface salinity on 1 March, 2019 using the original bathymetry, showing the salinity in the central delta is relative salty (over 10). The original bathymetry has a blockage in the CES, while the new bathymetry in CES is better connected. The difference in simulated surface salinity between using the modified and original bathymetry (Figure C2b) is negative in the central delta and part of the western delta, indicating that, using the modified bathymetry, freshwater can now flow into the river channel where TRN-05 is located, and other small streams in the CES, and as well as the river channels in the WES.

On the basis of the above comparison, the salinity simulations with both the original bathymetry and the modified bathymetry are validated using *in situ* salinity observations (Figure C3), to examine the direct impact of the original blockages on the river connectivity. In Figure C3a, the simulation with original bathymetry, the simulated salinity in western channels is slightly fresher than the observation, around 2 lower, and in the central channels are much smaller than observation by up to 8, but in the eastern channel the simulated salinity is much higher than observed. By removing all the blockage points (Figure C3b), the salinity simulation in the eastern channel is much improved through removing the blockage in the upper stream. However, the simulated salinity in the central channels is even smaller than the original simulation, with larger bias of over 10 at most observation points, this much lower salinity is due to more freshwater flowing into the Gorai River after removing the blockages, apparently. The spatial distribution of salinity bias is in an obvious west-central-east variation pattern.

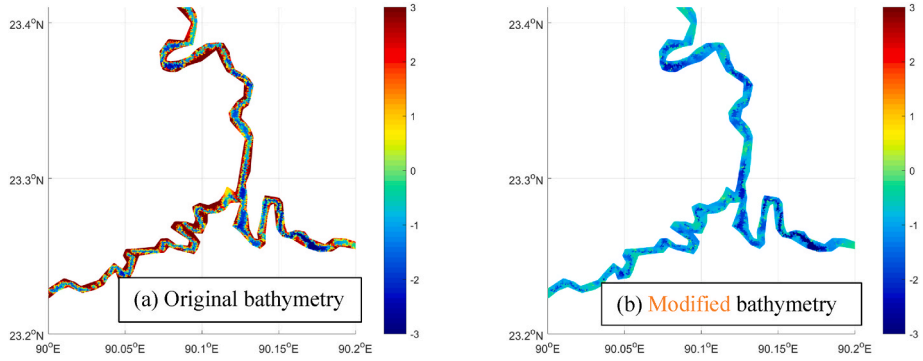

Fig. C1. Examples of the bathymetry modification, (a) before and (b) after.

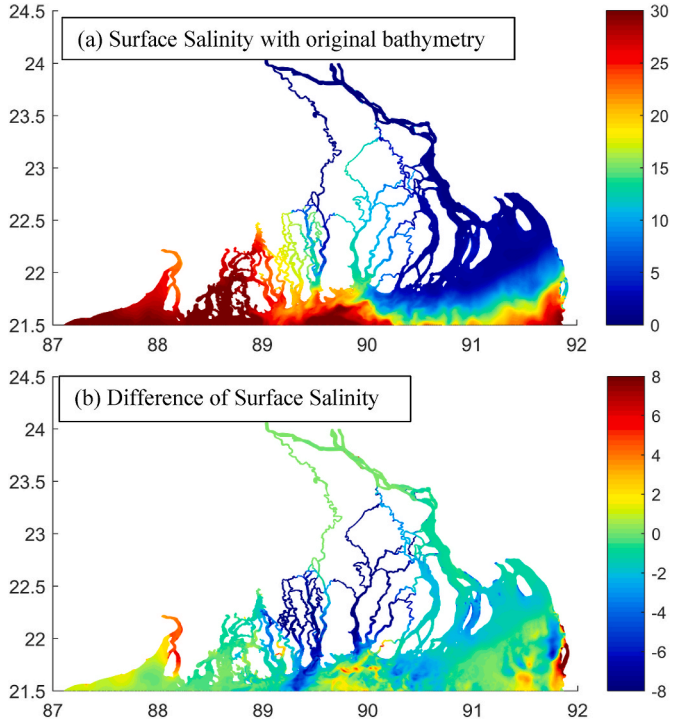

Fig. C2. Snap shot on 1 March, 2019 (a) surface salinity with the original bathymetry and (b) difference of surface salinity between the modified and original bathymetry.

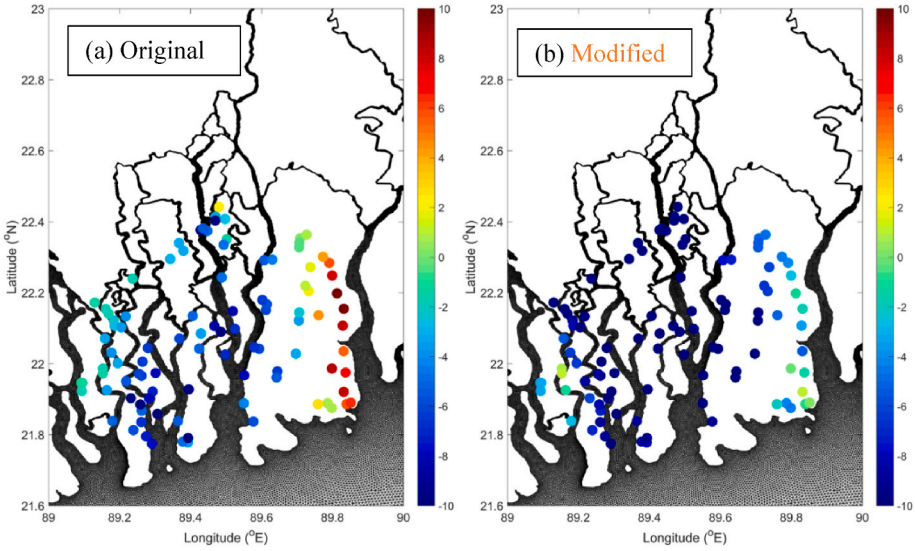

Fig. C3. Spatial patterns of Salinity differences between observations and simulations (a) with original bathymetry (b) with modified bathymetry.

References

Ahmed, N., Demaine, H., Muir, J.F., 2008. Freshwater prawn farming in Bangladesh: history, present status and future prospects. Aquacult. Res. 39, 806–819.

Akter, R., Asik, T.Z., Sakib, M., Akter, M., Sakib, M.N., Al Azad, A.S.M.A., Maruf, M., Haque, A., Rahman, Md M., 2019. The dominant climate change event for salinity intrusion in the GBM delta. Climate 7, 69. https://doi.org/10.3390/cli7050069.

Bowen, M.M., Geyer, W.R., 2003. Salt transport and the time-dependent salt balance of a partially stratified estuary. J. Geophys. Res. 108 (C5), 3158. https://doi.org/10.1029/2001JC001231.

Bricheno, L.M., Wolf, J., Islam, S., 2016. Tidal intrusion within a mega delta: an unstructured grid modelling approach. Estuar. Coast Shelf Sci. 182, 12–26.

Bricheno, L.M., Wolf, J., Sun, Y., 2021. Salinity intrusion in the Ganges-Brahmaputra-Meghna megadelta. Estuar. Coast Shelf Sci. 252, 107246. https://doi.org/10.1016/j.ecss.2021.107246.

Cea, L., French, J.R., 2012. Bathymetric error estimation for the calibration and validation of estuarine hydrodynamic models. Estuar. Coast Shelf Sci. 100, 124–132.

Egbert, G.D., Erofeeva, S.Y., 2002. Efficient inverse modeling of barotropic ocean tides. J. Atmos. Ocean. Technol. 19 (2), 183–204.

Elahi, M.W.E., Jalón-Rojas, I., Wang, X.H., Ritchie, E.A., 2020. Influence of seasonal river discharge on tidal propagation in the Ganges-Brahmaputra-Meghna delta, Bangladesh. J. Geophys. Res.: Oceans 125, e2020JC016417. https://doi.org/10.1029/2020JC016417.

Eslami, S., Hoekstra, P., Kernkamp, H., Trung, N.N., Duc, D.D., Quang, T.T., Februarianto, M., Dam, A.V., van der Vegt, M., 2019. Flow division dynamics in the Mekong delta application of a 1D-2D coupled model. Water 11, 837. https://doi.org/10.3390/w11040837.

Godin, G., 1972. The Analysis of Tides. University of Toronto Press.

Godin, G., 1999. The propagation of tides up rivers with special considenrations on the upper Saint Lawrence river. Estuar. Coast Shelf Sci. 48, 307–324.

Hale, R., Bain, R., Goodbred Jr., S., Best, J., 2019. Observations and scaling of tidal mass transports across the lower Ganges-Brahmaputra delta plain: implications for delta management and sustainability. Earth Surf. Dyn. 7, 231–245. https://doi.org/10.5194/esurf-7-231-2019.

Haque, A., Sumaiya, Rahman, M., 2016. Flow distribution and sediment transport mechanism in the estuarine systems of Ganges-Brahmaputra-Meghna delta. Int. J. Environ. Sustain Dev. 7 (1), 22.

Higgins, S.A., Overeem, I., Rogers, K.G., Kalina, E.A., 2018. River linking in India: downstream impacts on water discharge and suspended sediment transport to deltas. Elem Sci Anth 6, 20. https://doi.org/10.1525/elementa.269.

Horrevoets, A.C., Savenije, H.H.G., Schuurman, J.N., Graas, S., 2004. The influence of river discharge on tidal damping in alluvial estuaries. J. Hydrol. 294, 213–228.

Islam, S.N., 2016. Deltaic floodplains development and wetland ecosystems management in the Ganges-Brahmaputra-Meghna Rivers Delta in Bangladesh. Sustain. Water Resour. Manag. 2, 237–256. https://doi.org/10.1007/s40899-016-0047-6.

Jian, J., Webster, P.J., Hoyos, C.D., 2009. Large-scale controls on Ganges and Brahmaputra river discharge on intraseasonal and seasonal time-scales. Q. J. R. Meteorol. Soc. 135, 353–370.

Kawser, M.A., Samad, M.A., 2016. Political history of Farakka Barrage and its effects on environment in Bangladesh. Bandung J. Global South 3 (16). https://doi.org/10.1186/s40728-015-0027-5.

Kida, S., Yamazaki, D., 2020. The mechanism of the freshwater outflow through the Ganges-Brahmaputra-Meghna delta. Water Resour. Res. 56, e2019WR026412 https://doi.org/10.1029/2019WR026412.

Kosuth, P., Callède, J., Laraque, A., Filizola, N., Guyot, J.L., Seyler, P., Fritsch, J.M., Guimarães, V., 2009. Hydrol. Process. 23, 3141–3150. https://doi.org/10.1002/hyp.7387.

Kukulka, T., Jay, D.A., 2003a. Impacts of Columbia River discharge on salmonid habitat: 1. A nonstationary fluvial tide model. J. Geophys. Res. 108 (C9), 3293. https://doi.org/10.1029/2002JC001382.

Kukulka, T., Jay, D.A., 2003b. Impacts of Columbia River discharge on salmonid habitat: 2. Changes in shallow-water habitat. J. Geophys. Res. 108 (C9), 3294. https://doi.org/10.1029/2003JC001829.

Lellouche, J.M., Legalloudec, O., Regnier, C., Levier, B., Greiner, E., Drévillon, M., 2019. CMEMS-GLO-QUID-001-024, issue 2.1, E.U. Copernicus marine Service information [Online]. Available at: https://catalogue.marine.copernicus.eu/documents/QUID/CMEMS-GLO-QUID-001-024.pdf. (Accessed 4 February 2019).

Lerczak, J.A., Geyer, W.R., Chant, R.J., 2006. Mechanisms driving the time-dependent salt flux in a partially stratified estuary. J. Phys. Oceanogr. 36, 2296–2311.

Murshed, S.B., Rahman, M.R., Kaluarachchi, J.J., 2019. Changes in hydrology of the Ganges delta of Bangladesh and corresponding impacts on water Resources. J. Am. Water Resour. Assoc. 55 (4), 800–823. https://doi.org/10.1111/1752-1688.12775.

Papa, F., Durand, F., Rossow, W.B., Rahman, A., Bala, S.K., 2010. Satellite altimeter-derived monthly discharge of the Ganga-Brahmaputra River and its Seasonal to interannual variations from 1993 to 2008. J. Geophys. Res. 115, C12013. https://doi.org/10.1029/2009JC006075.

Papa, F., Bala, S.K., Pandey, R.K., Durand, F., Gopalakrishna, V.V., Rahman, A., Rossow, W.B., 2012. Ganga-Brahmaputra river discharge from Jason-2 radar altimetry: an update to the long-term satellite-derived estimates of continental freshwater forcing flux into the Bay of Bengal. J. Geophys. Res. 117, C11021. https://doi.org/10.1029/2012JC008158.

Rogers, K.G., Overeem, I., 2017. Doomed to drown? Sediment dynamics in the human-controlled floodplains of the active Bengal Delta. Elem. Sci. Anth. 5, 66. https://doi.org/10.1525/elementa.250.

Rosário, R.P., Bezerra, M.O., Vinzón, S.B., 2009. Dynamics of the saline front in the northern channel of the amazon river – influence of fluvial flow and tidal range (Brazil). Proceedings of the 10th International Coastal Symposium). J. Coast. Res. 56, 1414–1418. Lisbon, Portugal, ISSN 0749-0258.

Rynne Patrick, F., 2016. Observations and modeling of exchange and residence time in tidal inlets. Open access dissertations. Paper 1579.

Savenije, H.H.G., 2012. Salinity and Tides in Alluvial Estuaries. Second Completely Revised Edition. salinityandtides.com.

Savenije, H.H.G., Veling, E.J.M., 2005. Relation between tidal damping and wave celerity in estuaries. J. Geophys. Res. 110, C04007. https://doi.org/10.1029/2004JC002278.

Shaha, D.C., Cho, Y.K., 2016. Salt plug formation caused by decreased river discharge in a multi-channel estuary. Sci. Rep. 6, 27176. https://doi.org/10.1038/srep27176.

Shammi, M., Bhuiya, G.M.J.A., Kamal, A.K.I., Rahman, Md R., Rahman, Md M., et al., 2012. Investigation of salinity occurrences in Kumar-Madhumati river of Gopalganj District, Bangladesh. J. Nat. Sci. Sustain. Technol. 6 (4), 299–313.

Tazkia, A.R., Krien, Y., Durand, F., Testut, L., Islam, A.K.M.S., Papa, F., Bertin, X., 2017. Seasonal modulation of M2 tide in the northern Bay of Bengal. Continent. Shelf Res. 137, 154–162.

Wang, Z.B., Vandenbruwaene, W., Taal, M., Winterwerp, H., 2019. Amplification and deformation of tidal wave in the upper Scheldt estuary. Ocean Dynam. 69, 829–839. https://doi.org/10.1007/s10236-019-01281-3.

Whitehead, P.G., Sarkar, S., Jin, L., Futter, M.N., Caesar, J., Barbour, E., Butterfield, D., Sinha, R., Nicholls, R., Hutton, C., Leckir, H.D., 2015. Dynamic modelling of the Ganga river system: impacts of future climate and socio-economic change on flows and nitrogen fluxes in India and Bangladesh. Environ. Sci.: Process. Impacts 17, 1082–1097.

Whitehead, P.G., Jin, L., Macadam, I., Janes, T., Sarkar, S., Rodda, H.J.E., Sinha, R., Nicholls, R.J., 2018. Modelling impacts of climate changes and socio-economic change on the Ganga, Brahmaputra, Meghna, Hooghly and Mahanadi river systems in India and Bangladesh. Sci. Total Environ. 636, 1362–1372.

Winterwerp, J.C., Giardino, A., 2012. Assessment of Increasing Freshwater Input on Salinity and Sedimentation in the Gorai River System. Report to World Bank (Technical Report). Delft: Deltares. https://doi.org/10.13140/2.1.1504.1286.

Zhang, E.F., Savenije, H.H.G., Chen, S.L., Mao, X.H., 2012. An analytical solution for tidal dynamics in the Yangtze Estuary, China. Hydrol. Earth Syst. Sci. Discuss. 9, 2213–2244. https://doi.org/10.5194/hessd-9-2213-2012.

Zhang, W., Feng, H., Hoitink, A.J.F., Zhu, Y., Gong, F., Zheng, J., 2017. Tidal impacts on the subtidal flow division at the main bifurcation in the Yangtze River Delta. Estuarine. Coast. Shelf Sci. 196, 301–314.

Zhang, F., Sun, J., Lin, B., Huang, G., 2018. Seasonal hydrodynamic interactions between tidal waves and river flows in the Yangtze Estuary. J. Mar. Syst. 186, 17–28.